DRAFT

ES2019-3826

CHARACTERIZATION OF PARTICLE AND HEAT LOSSES FROM FALLING PARTICLE RECEIVERS

Clifford K. Ho,[1] **Sean Kinahan**
Sandia National Laboratories
Albuquerque, NM, USA

Jesus D. Ortega, Peter Vorobieff, Andrea Mammoli
University of New Mexico
Albuquerque, NM, USA

Vanderlei Martins
AirPhoton
Baltimore, MD, USA

ABSTRACT

High-speed visible and infrared cameras were evaluated to quantify both particle and convective heat losses from the aperture of a high-temperature particle receiver. A bench-scale system replicating the on-sun particle receiver was built, and particle velocities and temperatures were recorded using the small-scale system. Particles heated to over 700 °C in a furnace were released from a slot aperture and allowed to fall through a region that was imaged by the cameras. Particle-image, particle-tracking, and image-correlation velocimetry methods were compared against one another to determine the best method to obtain particle velocities. The high-speed infrared camera was used to evaluate particle temperatures, and a model was developed to determine particle and convective heat losses. In addition, particle sampling instruments were deployed during on-sun testing of the particle receiver to determine if small particles were being generated that can pose an inhalation hazard. Results showed that while there were some recordable emissions during the tests, the measured particle concentrations were much lower than the acceptable health standard of 15 mg/m^3. Additional bench-scale tests were performed to quantify the formation of particles during continuous shaking and dropping of the particles.

INTRODUCTION

Particle receivers are being pursued to enable higher temperatures (>700 °C) and greater power cycle efficiencies (≥50%) for concentrating solar power (CSP) plants [1]. Small sand-like particles fall through a receiver and are heated by a beam of concentrated sunlight. The hot particles can be stored and used when needed for electricity production, process heating, thermochemistry, and solar fuels production. Sandia National Laboratories has previously demonstrated a 1 MW$_t$

high-temperature falling particle receiver system that has achieved particle temperatures over 700 °C [2-4]. The ceramic particles (from CARBO Ceramics) were composed of sintered bauxite and were ~200 – 400 microns in size. Findings from that study indicated that direct irradiance of falling particles enabled very high heating rates of the particles, but additional methods to reduce heat losses (convective and radiative) and particle losses are needed to increase receiver thermal efficiencies, reduce costs, and mitigate potential health risks from inhalation of fine particles.

This paper summarizes imaging methods to characterize the particle and heat losses during on-sun operation of the falling particle receiver. In addition, particle sampling and air-monitoring instruments were deployed during on-sun tests to provide exposure assessments for particulate matter inhalation safety risks.

PARTICLE IMAGING

Camera-based imaging methods were evaluated to perform in-situ measurements of particle loss from the high-temperature particle receiver. The temperature of the particles was also desired so that estimates of the convective heat loss from the receiver aperture could be determined using the particles as an advective tracer.

Imaging Requirements and Tools

Alternative imaging methods were evaluated and assessed based on the desire to measure particle velocities (up to ~5 m/s) and temperatures (up to ~700 – 800 °C) in a dilute plume of illuminated particles. Methods included visible and infrared cameras, two-wavelength pyrometry with particle luminescence, and laser-beam scattering. Features and requirements of the imaging ssytem are summarized in Table 1 based on an

---

[1] Contact author: ckho@sandia.gov

evaluation of the anticipated processes and scenarios during particle ejection from the receiver aperture. The distance between the imaging system and the receiver aperture will be ~4 – 6 m, and the field of view needs to be ~1 m² to capture particles escaping the ~1 m² receiver aperture. The resolution and frame rate requirements are driven by the movement of ~100 – 400 micron particles at up to ~5 m/s. Additional considerations include the effect of concentrated sunlight reflecting off the particles, which may confound the spectral measurement of radiation in the visible and near-infrared bands. The system also needed to be rugged and less than ~$100K. Based on these requirements, camera-based imaging systems were selected. The IR camera selected was the InfraTec Thermographic system ImageIR® 8320 HP (Figure 1) which operates at 355 frames per second (up to 1,200 quarter frames per second) with a resolution of 640x512 IR pixels and a thermal resolution of 0.02 K.

Table 1. Requirements for camera selection.

Feature	Requirement	Basis
Field of View	1 m²	Aperture Size of Particle Receiver
Focal Length	100 - 250 mm	Based on distance away from the aperture and resolution
Resolution	> 480 pixels (640x512)	Need sufficient resolution to track particle motion and velocities up to ~5 m/s (particle falling speed)
Frame Rate	> 900 fps (to capture 5 mm movement at 5 m/s max particle speed)	Proportional to the resolution of the camera and the velocity of the particles. Assumed that the velocity of the particles ejected from the receiver are <5 m/s (free fall speed).
Spectral range	Visible (0.4-0.78 microns) IR (2-4 microns)	Filtering required to reduce the intensity of the incident light on the curtain
Cost	< ~$100K	Cannot exceed budget
Ruggedness	Must withstand outdoor environments with particles	Need to ensure that camera(s) are weather-resistant and particle proof, or a hood/housing is constructed to protect the camera from the particles and irradiance.

Imaging Methods for Particle Velocities

The velocity distribution of the particles can be obtained by several techniques including particle image velocimetry (PIV), particle tracking velocimetry (PTV), and image correlation velocimetry (ICV). A high-speed camera is necessary to capture data at the required rate to have an appropriate postprocessing. This work focused on one technique for characterizing the flow of the curtain: advection corrected correlation image velocimetry (ACCIV). ACCIV is directly related to PIV; it is a system for tracking the movement of particles between sequences of images to determine the velocity distribution of the falling curtain. The

main difference between PIV and ICV is that PIV tracks translation of particle clusters, while ACCIV tracks a greater variety of flow features such as density pockets (in this case, agglomerated clusters of particles) undergoing translation, rotation, and dilation. In addition to feature tracking, ACCIV uses the advection equation to help remove the uncertainties inherent in the automated process [5]. Results from ACCIV analysis are interpolated and smoothed using a multilevel B-spline adaptive algorithm [6]. The output from ACCIV represents the velocity distribution of the particles in the falling curtain.

Figure 1. InfraTec thermographic system ImageIR® 8320 HP with 100 mm lens

Imaging Methods for Particle and Heat Losses

The particle and advective heat losses from an open aperture of a falling particle receiver can be estimated through an energy balance equation, which requires parameters obtained from the imaging methods described in the previous section. If we consider advective energy flows in and out of the particle receiver control volume, the following energy balance can be written:

$$Q_{loss} = \dot{m}_p \left(h_{p,out} - h_{p,in} \right) + \dot{m}_a \left(h_{a,out} - h_{a,in} \right) \qquad (1)$$

or

$$Q_{loss} = \dot{m}_p \bar{c}_p \left(T_{p,out} - T_{p,in} \right) + \dot{m}_a \left(h_{a,out}(T_{a,out}) - h_{a,in}(T_{a,in}) \right) \qquad (2)$$

where Q_{loss} is the rate of advective energy loss (W) from the particles and air, $\dot{m}$ is the mass flow rate (kg/s), $\bar{c}_p$ is the specific heat of particles evaluated at the average of the inlet and outlet temperatures (J/kg-K), T is the temperature (K), h is the

enthalpy (J/kg), p denotes particles, a denotes air, and *in* and *out* denote the state of the material entering or leaving the receiver aperture. In the case of particles, the state of particles entering the receiver is assumed to be at ambient for the purposes of heat loss determination. For air, the temperature of the entering air will be assumed to be equal to the outside ambient temperature, and the temperature of the air leaving the receiver will be measured using radiation-shielded thermocouples located inside the receiver just above the aperture.

The air mass flow rate in Eq. (2) is calculated as follows:

$$\dot{m}_a = \rho_a(T_a)v_a A_{flow,a} \qquad (3)$$

where ρ_a is the air density that can be calculated based on a measured air temperature leaving the aperture, v_a is the air velocity (m/s), and $A_{flow,a}$ is the cross-sectional area of air flow (m^2). The air velocity and cross-sectional flow area will be assumed equal to the particle velocity and particle flow area described in Eq. (4). Although not exact, it will provide a first approximation. The particle mass flow rate, $\dot{m}_p$, can be expressed as follows:

$$\dot{m}_p = \rho_{b,p} v_p A_{flow,p} \qquad (4)$$

where $\rho_{b,p}$ is the bulk particle density (kg-particle/m^3-total), v_p is the particle velocity (m/s), and $A_{flow,p}$ is the cross-sectional area of particle flow (m^2). The particle velocity is obtained from the camera imaging methods described previously, and the particle flow area can be estimated from the receiver aperture size and visible particle flow in the images. The bulk particle density can be determined from the product of the intrinsic particle density, ρ_p, and the particle volume fraction, f_p (m^3-particles/m^3-total):

$$\rho_{b,p} = \rho_p f_p \qquad (5)$$

The particle volume fraction, f_p, can be determined by a modified version of Beer's law describing the attenuation (transmittance) of radiation caused by the presence of a curtain of particles with thickness, w (m), and particle diameter, d_p (m) [7]:

$$\frac{I}{I_o} = e^{\frac{-3f_p w}{2d_p}} \qquad (6)$$

or

$$f_p = -\frac{2d_p \ln\left(\frac{I}{I_o}\right)}{3w} \qquad (7)$$

where I and I_o are the attenuated and unattenuated irradiance (W/m^2), respectively. The transmittance of the background radiation through the particles ejected from the aperture can be determined from the ratio of the pixel values in camera images with and without particles in the field of view [8]. The particle flow system can be periodically shut off to obtain the reference image without particle flow. The camera pixel values represent the irradiance values in Eqs. (6) and (7). It should be noted that if an IR camera is used, post-processing of the images may be required to utilize the thermal-based irradiance values.

The temperature of the particles will be measured with the InfraTec IR camera. A challenge is that each pixel of the camera sensor may "see" both particles and background in the field of view. As a result, calibration of the prescribed particle emissivity used by the IR camera may be needed to get accurate particle temperature measurements. Alternatively, the particle temperature may be obtained during laboratory testing by using thermocouple measurements of the particles before and after they are released along with a lumped capacitance model of particle heat transfer to interpolate the particle temperatures. Both methods are described below.

Emissivity Calibration Method. A simple calibration method will be tested that determines a suitable camera-based emissivity value that will yield accurate particle temperatures measured from the IR camera. The thermal radiation received by the camera sensor will be from both the particles and the background within the field of view. In the lab tests, the background may be the walls or protective panels. In the on-sun tests, the background may be the sky or a fabricated panel above the receiver. During the laboratory tests, a water-cooled panel can be installed that can be temperature controlled. Using different prescribed camera emissivities, we can see which emissivity as a function of background temperature and/or solids volume fraction yields the most accurate particle temperatures when compared to the interpolated temperatures from the thermocouple readings at the inlet/outlet and the lumped-capacitance model (see below). The impact of background temperature background temperature can be extrapolated to determine which camera emissivity to use during on-sun tests when the background is the sky or a temperature-controlled panel above the receiver to serve as the "background".

Lumped-Capacitance Method. The lumped-capacitance energy-balance for a single particle assumes that each particle is isothermal (Biot number ≤ 0.1), and an effective heat transfer coefficient, h (W/m^2-K) describes the heat loss from radiation and convection while falling. The particle temperature is expressed as an exponentially decaying function of time, t (s). Using the measured temperatures at the inlet and outlet of the falling-particle bench-scale test (representing the initial and final particle temperatures during its fall), the heat transfer coefficient can be used to generate temperature profiles that fit the data. In turn, this can be used to obtain particle temperatures as a function of position. The interpolated particle temperatures at each location can then be used with the camera-measured pixel temperature, which includes contributions from both the particle and background radiative emittance, to determine the particle area and volume fractions.

The normalized particle temperature as a function of time resulting from the lumped-capacitance energy balance can be expressed as follows:

$$T_{norm} = \frac{T_p(t) - T_{amb}}{T_p(t=0) - T_{amb}} = \exp\left[-\left(\frac{hA_p}{\rho_p V_p c_p}\right)t\right] \qquad (8)$$

where V_p and A_p are the volume and surface area of the particle, T_{amb} is the ambient temperature and the ratio can be expressed as $d_p/6$ for a sphere, where d_p is the particle diameter (m). Eq. (8) is used to fit a heat-transfer coefficient, h, to match the initial and final temperatures of the falling particles.

Once the heat-transfer coefficient has been determined, the particle temperature at any time can be used to determine the particle temperature as a function of position between the starting and ending points using equations to approximate the free fall of particles [8]. The particle temperature can be used together with the camera-measured temperature of each pixel to estimate the projected particle area fraction in the image, which can then be used to estimate the particle volume fraction to determine the particle mass flow rate and bulk density in Eqs. (4) and (5). The particle projected area fraction, α_p (m²-particle/m²-total), can be estimated based on an energy balance for each pixel, which is comprised of thermal radiation from any particles in the field of view plus radiation from any emitting background material:

$$\varepsilon_{px} A_{px} T_{px}^4 = \varepsilon_b A_b T_b^4 + \varepsilon_p A_p T_p^4$$

or
$$\varepsilon_{px} T_{px}^4 = \varepsilon_b \left(1 - \alpha_p\right) T_b^4 + \varepsilon_p \alpha_p T_p^4 \qquad (9)$$

where ε is the emissivity, A is the area (m²), and T is the temperature (K). The subscripts, $px, b,$ and p denote pixel, background, and particles, respectively. Eq. (9) can be used to solve for the particle area fraction, α_p, which, assuming the particles are opaque, also equals the opacity. Opacity can be expressed as follows using Beer's law [7]:

$$opacity = \alpha_p = 1 - \frac{I}{I_o} = 1 - e^{\frac{-3 f_p w}{2 d_p}} \qquad (10)$$

Eq. (10) can be used to solve for I/I_o using the particle area fraction, α_p, from Eq. (9). The solids volume fraction, f_p, can be solved using Eq. (7), which enables solution of the bulk particle density and mass flow rate in Eqs. (5) and (4).

Particle Imaging Testing

A lab-scale experiment was constructed to test the imaging methods (Figure 2). Particles heated in a furnace up to ~700 – 800 °C are released onto a screen mesh that accumulates particles over a K-type thermocouple for initial temperature measurement. The particles move downward through the mesh and fall through a region (~36 cm in height) that is imaged by the IR camera, which was located approximately 5 meters away to replicate the on-sun testing conditions. The particles fall into a collection bin that is weighed to determine the particle mass flow rate. A K-type thermocouple is located in the collection bin to measure the outlet temperature of the particles. An Arduino Mega microcontroller is used to collect data from the thermocouples and load cells for temperature and mass flow measurements.

An initial test was performed with particles heated to ~500 °C. The IR camera collected thermal images of the falling particles at a frame rate of 300 fps. The ACCIV methodology was used to to obtain the velocity field and contours from the thermal images of the falling particles (Figure 3). To validate the results from ACCIV, the values were compared to the results obtained using standard PIV methodology with the same data set. Both methods yielded similar vertical velocities throughout the falling particle curtain.

Future tests will evaluate the ability of the IR camera to measure the particle temperatures using both the emissivity calibration method and the lumped-capacitance modeling method described earlier. In addition, a solar simulator is being constructed to understand the impacts of concentrated light on the thermal imaging techniques to measure particle temperatures. Estimation methods of particle and heat losses will be assessed, and a final algorithm for on-sun testing will be developed.
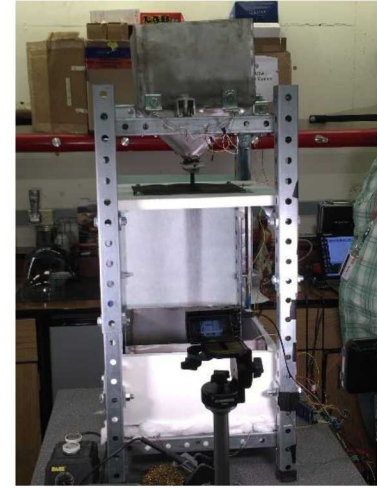

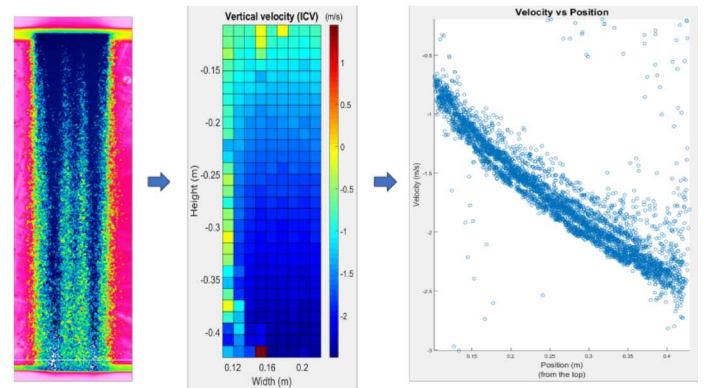**Figure 2. Lab-scale experiment to evaluate imaging methods.**

Figure 3. Extracting velocity data from thermal images using ACCIV.

PARTICLE SAMPLING FOR EXPOSURE ASSESSMENT

Lab Testing of Particle Attrition and Generation

A series of laboratory experiments were conducted to separate and characterize the generation of small particles (<10μm) during particle agitation. Small particles are produced by deagglomeration, abrasion and fracture from the larger particle components due to attrition. Both shaking and dropping methods were tested to evaluate the production of small particles using CARBO HSP 40/70 ceramic particles (Figure 4).

In the shaking method, the particle shaker is constantly vibrating the particles at a constant frequency and amplitude, while clean air flushes particles to a cyclone separator that can be tuned to different particle cut-off sizes. The constant particle shaking provides attrition between the particles and produces the deagglomeration of small particles as well as the abrasion and fracture of larger particles into smaller fragments.

In the dropping method, particles are slowly dropped inside a tube from a height of about 1.2 m while being flushed by a constant flow of clean air. The air flow drags the small particles to a cyclone separator where particles are size selected between 1 to 10μm aerodynamic diameters. The aerodynamic diameter is defined as the diameter of the sphere with unit density that has the same settling velocity as the particle being measured.

Results showed continuous production of small particles in two size ranges: less than 1.3 μm and between 7.5 and 10 μm (aerodynamic diameter). These particles are likely produced by the attrition, fracture and abrasion of the parent CARBO particles. Figure 5 shows optical and scanning electron microscopy (SEM) images of the original particles and generated particles during the shaking/dropping tests. We postulate that the small generated particles (<1 μm) were pre-existing and were attached to the larger parent particles. The small particles can be created during the original manufacturing of the CARBO particles from combustion, gas-to-particle conversion, or molecular nucleation. The deagglomeration of these small particles from the parent particles was caused by collisions during shaking or dropping of the particles. The larger particles (~8 – 10 μm) are produced from mechanical fracturing or abrasion of the original particles. Initial estimates of the generation rate for particles in both size ranges is ~$1.4\text{x}10^{-5}$ % of the original mass of the particles per drop inside the laboratory column.

On-Sun Testing and Particle Sampling

On April 5, 2018, Sandia's aerosol team deployed a wide range of sampling instrumentation for sub and super-micron particulate monitoring to the solar tower to investigate accidental particle release when operating the falling particle receiver. The goal of this testing was to look for smaller particulates that may cause fouling of heliostats, release into the environment, or an impact to human health. Instrumentation included a Scanning-Mobility Particle Sizer (SMPS), Aerodynamic Particle Sizers (APS), DustTraks, SKC AirChek Personal Samples, Dry Filter Units, and a Malvern Spraytec.
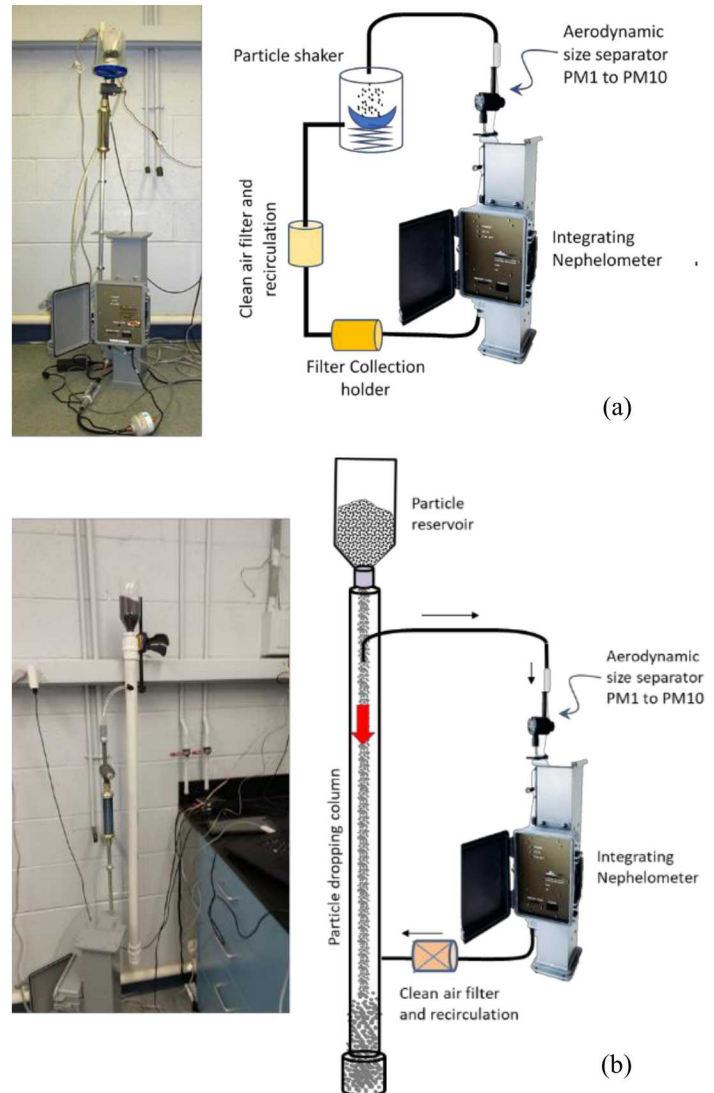

(a)

(b)

Figure 4. Two methods to evaluate particle attrition and generation of small particles: particle shaker (a) and dropping column (b).
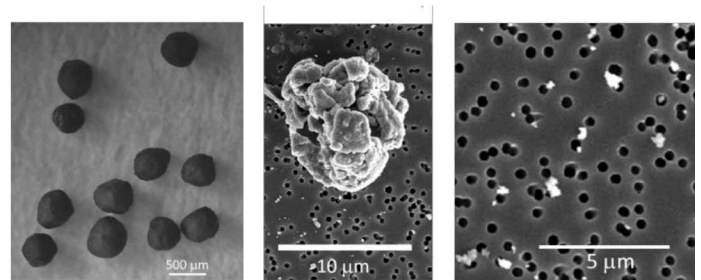

Figure 5. Optical microscopy image of the original particles (left) and SEM images of generated particles (which appear white in the center and right images).

5

© 2019 by ASME

The Dry Filter Units and Personal samplers collect onto filters for offline analysis, whereas the other instruments analyze samples in real time. The Personal Samplers followed NIOSH sampling procedure 0500 the standard for exposure to "particulates not otherwise regulated, total [9]." In this reference, the term total indicates that this procedure does not use sampling techniques to limit the sample to respirable particles that deposit deep within the lungs, and therefore integrates the mass exposure over a broader size range. The overall approach utilizes gravimetric weighing of filters, with exposure limits tied to the OSHA standard of 15 mg/m^3.

For real-time instrumentation, the SMPS utilizes electric mobility of small particles to determine submicron concentrations (~10 to 600 nm) that could be created as part of the heating and processing of ceramic particulate. The APS utilizes time-of-flight to determine the aerodynamic diameter of a particle, based on how long it takes a particle to travel between two laser beams. This method of sizing is inherently more valuable to aerosol modeling for a particle's delivery in the lungs or environment, since it is inherently measuring the aerosol physics of the particle, and not just the geometric physical diameter. The Malvern Spraytec utilizes laser diffraction to size very large particles (up to 2000 microns) and droplets in a given field of view. Lastly, the DustTrak instruments measure total PM10, which is defined as particulate matter up to 10 microns in diameter. This definition is intended to include the respirable range of particles, and is an EPA pollution standard, as opposed to an occupational health standard.

As shown in Figure 6, most instruments were placed at the top of the tower, closest to the point of generation, but instruments were also placed at the base of the tower. Figure 7 and Figure 8 show images of the instruments and their placement.

For offline analysis of filter samples, three types of filter weights were included. A pre-testing background set of filters taken before testing, integrated weights collected during all particle receiver testing, and a post-testing background filter. All personal sampler filters, which were collected for a minimum of 30 minutes, and weighed at the microgram sensitivity level, lost a small amount of weight (an average of 77 micrograms, n=7), except for the filter collected in location 3, on the particle receiver platform, to the South-East of the receiver. With wind coming from the North-West, this filter was directly downwind, and had a few visible ceramic beads loaded onto the filter. This filter increased in weight by 88 micrograms. For a filter collecting at 2 liters per minute for 75 minutes (per NIOSH NMAM 0500), this corresponds to 88 micrograms per 150 liters, or 0.586 mg/m^3, well below the limit for exposure (15 mg/m^3).

1) Top of Manlift – 1 APS, 1 Malvern (AM), 1 DustTrak.
2) Base of Particle Receiver – 1 APS, 1 DustTrak, 1 SMPS, 1 SKC (NIOSH) Sampler (AM)
3) SE Corner of Platform – 1 DFU, 1 Malvern (PM), 1 SKC (NIOSH) Personal Sampler (PM)
4) Ground Level SW of Tower – 1 DFU (AM), SKC (NIOSH) Sampler (AM), DustTrak (AM)
5) Ground Level SE of Tower – DFU (PM), SKC (NIOSH) Sampler (PM), DustTrak (PM)

Figure 6. Plan view of instrument placement at solar tower on April 5, 2018. Winds were from the north/northwest at ~5 – 10 mph (gusts up to 20 – 30 mph).

Real-time data gives a better picture of what actions on the tower caused any incidental aerosolization, including possible causes and the resulting size distributions. This data can be captured a few ways, including the number of particles of a particular size per volume of air, or as a mass, which ties to both NIOSH and EPA regulations via assumptions on measured particles being spherical, and having a given aerosol density. To look at what events cause aerosolization, the team first examined integrated concentration for a given instrument versus time, to look for spikes in aerosolization compared to background.

In Figure 9, which includes both sub-micron SMPS and super-micron APS results, data before 10:50 represents background aerosol concentrations from before testing began, and data after 13:39 is background for after testing concluded. As is mentioned in the figure description, the yellow stars represent times when the particle receiver was started, green stars represented times when the weigh hopper was activated, and blue stars represented the termination of the particle receiver.
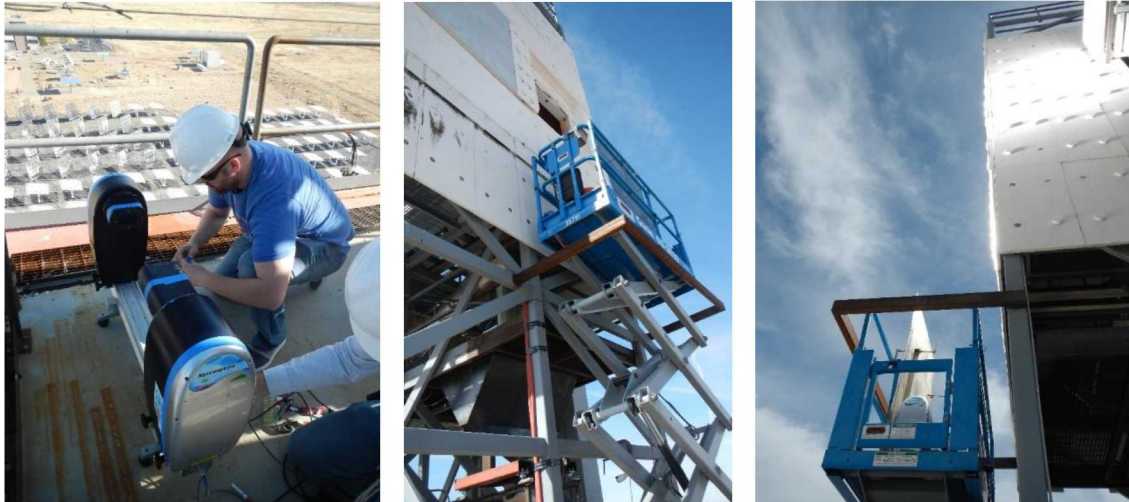
Figure 7. Images of the Malvern Spraytec used to evaluate large particle emissions (tens to hundreds of microns). The Spraytec was placed in an aerial lift to be positioned just beneath the aperture of the receiver.
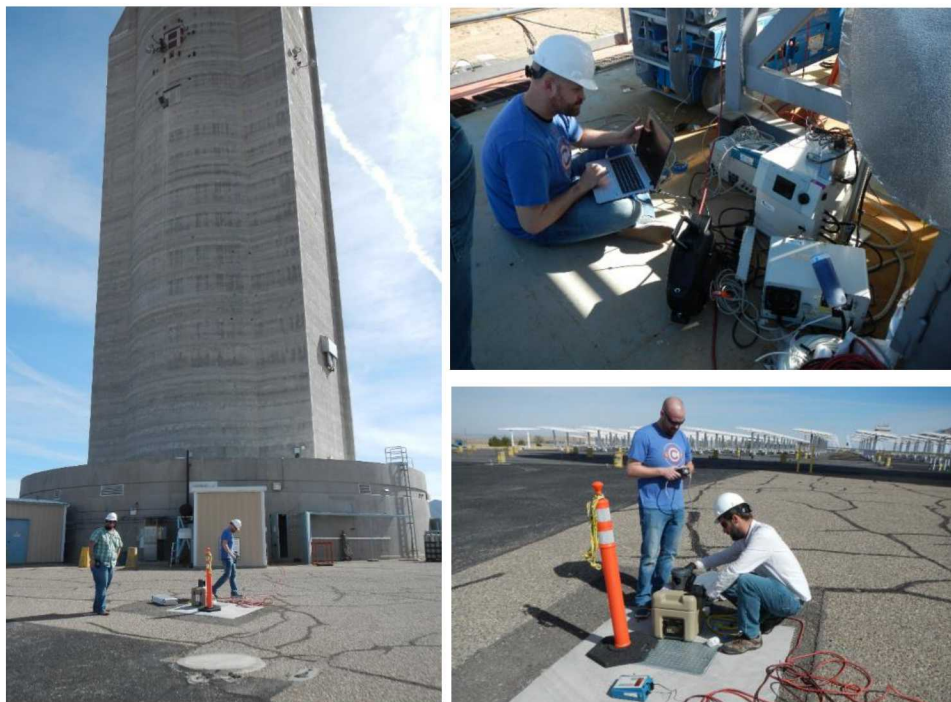

Figure 8. Setting up traditional volumetric air samplers to evaluate small particle emissions (submicron to micron) at the base and top of the tower.

A few key takeaways, before investigating the particle-size distributions and mass concentrations at specific timepoints, are as follows: First, there is not consistent aerosolization occurring in the super-micron (respirable) range when the receiver is operating (red, blue, yellow, and orange lines). Instead, there are only very transient spikes in concentration associated with startup or shutdown. Second, those concentration spikes were strongest the first time a system was activated, including the

overall particle receiver, and the weigh hopper. Subsequent activations during the same day saw decreased aerosolization. This could be verified visually as well, with a cloud of small particulate present when, for example, the weigh hopper was first activated. A likely reason for this to be occurring is that initial operation re-aerosolized ambient desert dusts that had collected in the receiver and on the ceramic spheres, with less re-aerosolization occurring throughout testing. If these super-

micron aerosols were being actively created, the concentration would be more consistent, and not decreasing over time.
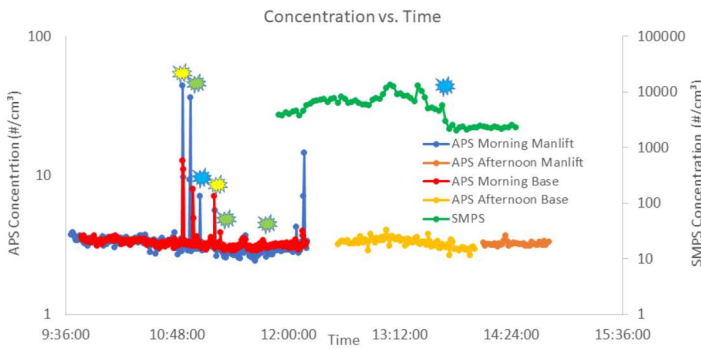

Figure 9. Aerosol Concentration versus Time. Yellow stars represent turning the particle receiver on, green stars represent the activation of the weigh hopper, and blue stars represent termination of particle receiver operations.

The SMPS (green data points in Figure 9) was not initially operating at the solar tower, but began operating after troubleshooting at 11:53 AM. As discussed above, this instrument measures sub-micron aerosols, which are both higher in concentration and more naturally fluctuating than the super-micron particulate measured by the APS. However, despite the variations in the concentration at the top of the solar tower, it does appear that the concentration during particle receiver testing (before 13:39) is substantially higher than after the receiver was turned off (after 13:39). There was a drop-in concentration of approximately 50%, with counts going from 4500 to 2166 particles per cubic centimeter after the receiver was stopped. It is unclear from the real-time data what could be causing this sub-micron particle generation, as it could be a result of the moving parts in the receiver itself, or from the ceramic particulate.

Since real-time data is taken at a high resolution, it is possible to evaluate the distributions at each time-point of interest, for instance when the receiver is first activated, to see if larger or smaller particles are being generated, or if it is just the total concentration that has changed.

If we take a slice of the integrated concentration timeseries above (Figure 9), and examine the size distributions by mass concentration, a couple takeaways become clear (Figure 10). First, the mass concentrations are low, even during spikes in concentration. The largest spike, in blue below, corresponds to the first time the receiver was activated, and integrates to only 2.577 µg/m3, and occurred transiently before quickly returning to baseline. The same trend in additional activations having a reduced concentration of particles can be seen in the green curve below, when the receiver was started for a second time. The magnitude of this distribution is reduced from the initial activation, indicating that re-aerosolization of background dusts occurs, and not that a consistent aerosolization process occurs whenever the receiver is started.

Second, when spikes in aerosol concentration occur, the particulates are larger in both quantity and diameter. There are multi-modal distributions with multiple peaks between 2 and 10 microns that are not present in background samples across all of the spiked aerosol concentrations in Figure 10.
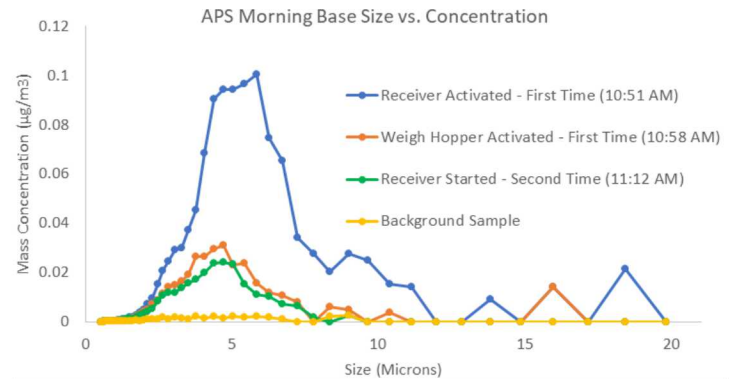

Figure 10. Aerosol Size Distribution by Mass. Mass distributions for several transient spikes that occurred during testing in conjunction with specific test events, such as activation of the particle receiver or weigh hopper.

The DustTrak instrumentation, offered somewhat similar insights, with less resolution in sizing (Figure 11). In agreement with the filter measurements, there was no substantial mass at the base that corresponded to a testing related activity, with most noticeable spikes occurring at the top of the tower, and early in testing.
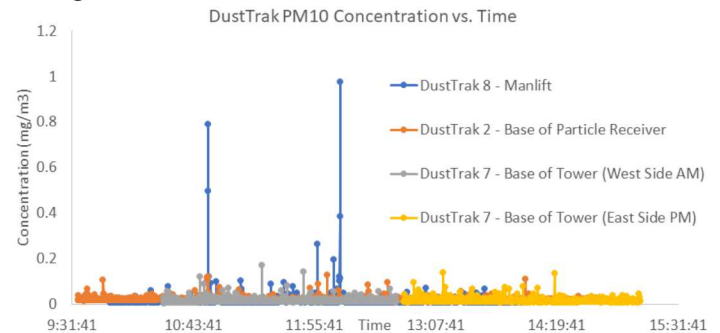

Figure 11. Dustrak PM10 Concentration versus Time.

The Manlift DustTrak (Blue in Figure 11) saw a similar spike when the particle receiver was activated for the first time that day (10:52 AM), with a smaller spike also observable in the instrument located at the base of the particle receiver. Similar to the APS, both instruments see a much smaller spike in concentration at 10:59-11:00, when the weigh hopper is first activated. At 12:10 pm, the manlift was re-arranged, and explains the sudden increase in particulate, which is not a result of the particle receiver testing. After the first few well-correlated increase in particle concentration, the data became noisier, likely as wind picked up, and sudden spikes in concentration were much smaller, and not correlated to testing events.

8

The team is pursuing methods of further processing offline collected filters to determine particle size and composition, with the potential benefits being a better understanding of what particles were generated in the spikes in real-time data, and whether they are naturally occurring or from the ceramic beads. Two approaches are being considered. The first is inductively coupled plasma mass spectrometry (ICPMS), which utilizes an acid rinse to extract filters, and then a low ppb examination of the inorganic makeup of the collected material. Because the beads are predominantly silica and alumina, which occur naturally, titanium oxide is the compound most expected to differentiate between naturally occurring and ceramic materials. Potential drawbacks could include a high limit of detection, since aerosolization was brief, and filters are likely to contain little material, and potentially interference or destruction from the acid wash preparation.

Alternatively, the team is investigating Scanning Electron Microscopy / Energy Dispersive X-Ray Spectroscopy (SEM/EDS) which has a significantly higher limit of detection (ppm) but can visualize particles on filters (to determine size and shape), and determine the inorganic makeup at specific locations on the filter, which may help with the limit of detection. Visualization alone may help determine between desert dust and ceramic material.

In both cases, control filters that have been doped with desert dust and ceramic bead dust will first be analyzed, to ensure that the methodology works, and limits of detection are sufficiently low. Then real-world samples would be utilized, with additional filters collected if necessary.

The Malvern Spraytec was intended to measure large (~100 micron) particles that exited the particle receiver through the aperture. It uses laser particle diffraction across between transmitter and receiver optical windows to determine size of droplets or particles up to 1000 microns in size. This size range is substantially larger than the exposure and environmental aerosol instrumentation analyzed above. The instrument measures the sphere-equivalent volume of particles in the frame, but this can be converted to a number or mass concentration.

For most of the day, the instrument reported few large particles passing through the view of the instrument, except when they were manually dropped for demonstration purposes. There are a few reasons the instrument may not see particulate. First, the instrument takes a background of naturally occurring particles for subtraction and looks for consistent signal above background to count a particle. This can mean that it takes more than a few particles to generate enough signal to be counted. The sensitivity was adjusted lower, which can mean noisier data, to examine whether any particulate fell in front of the receiver. The likelihood of noise is reduced by the very large ceramic bead size, and lack of naturally occurring particles in this range. Additionally, as stated above, placement in a turbulent environment dominated by wind factors means placement is key, and likely to result in wide variations in the number of particles. There were no particles in the morning on the man-lift, but there were some seen during the afternoon, when the instrument was

on the SE corner of the building, downwind and lower than the receiver.

Figure 12 shows the particle size distribution of particles that were manually dropped in front of the receiver. The particles align closely with the size distribution of beads purchased, with a mean size of 396 microns, indicating that the Malvern Spraytec was operating properly, and that continuous stream of large particle releases were not observed.
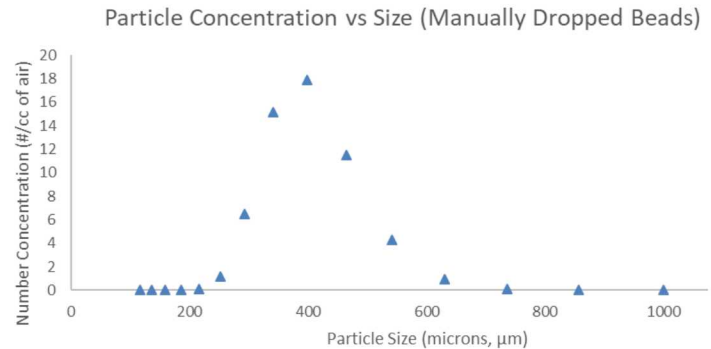

Figure 12. Particle size distribution of CARBO HSP 40/70 mesh particles measured by the Malvern Spraytec.

CONCLUSIONS

This paper described methods to characterize the mass flow and temperature of particles emitted from the aperture of a high-temperature falling particle receiver. A requirements table was created for the particle-imaging methods, and various in-situ methods and tools were evaluated. An InfraTec IR camera was selected based on it high resolution and frame rate. A bench-scale test and procedures were developed to assess the imaging methods. Thermal images collected from the IR camera were used to determine the particle velocity and temperature, and an algorithm was derived that determines the advective heat loss from the receiver aperture. Ongoing work will refine the imaging methods to develop a technique that can be used to characterize particle and advective heat losses during on-sun tests.

Both laboratory and on-sun field tests were conducted to evaluate the generation of small particles. Results of laboratory tests showed that a continuous generation of fine particles ($< \sim 1$ μm) was observed and likely caused by a deagglomeration of fine particles attached to the parent particles during production processes. Generation of larger particles ($\sim 8 - 10$ μm) was likely due to mechanical fracturing and abrasion processes during the continuous shaking and dropping. The generation rates of small particles in these sizes was estimated to be $\sim 1.4 \times 10^{-5}$ % of the original mass of the particles per drop inside the laboratory column.

However, field tests did not reveal an exposure hazard to small particles during on-sun particle receiver tests. A variety of air sampling instruments were deployed near the receiver and at the base of the tower. Results from these field tests showed that

while there were some recordable particle emissions from the testing, the particle concentration limits were much lower than acceptable health standards of 15 mg/m^3. Most of the recorded emissions were suspected to be from start-up events that emitted dust accumulated on equipment. Ongoing tests are being performed to determine if the composition of the collected particles is from indigenous soils or from the ceramic particles.

ACKNOWLEDGMENTS

REFERENCES

[1] Ho, C.K., 2016, A Review of High-Temperature Particle Receivers for Concentrating Solar Power, *Applied Thermal Engineering*, **109**(Part B), p. 958-969.

[2] Ho, C.K., J.M. Christian, J. Yellowhair, K. Armijo, and S. Jeter, 2016, *Performance Evaluation of a High-Temperature Falling Particle Receiver*, in *ASME Power & Energy Conference*, Charlotte, NC, June 26-30, 2016.

[3] Ho, C.K., J.M. Christian, J. Yellowhair, S. Jeter, M. Golob, C. Nguyen, K. Repole, S.I. Abdel-Khalik, N. Siegel, H. Al-Ansary, A. El-Leathy, and B. Gobereit, 2017, *Highlights of the High-Temperature Falling Particle Receiver Project: 2012 - 2016*, in *SolarPaces 2016: International Conference on Concentrating Solar Power and Chemical Energy Systems*, Abu Dhabi, UAE, October 11 - 14, 2016.

[4] Ho, C.K., J.M. Christian, J. Yellowhair, N. Siegel, S. Jeter, M. Golob, S.I. Abdel-Khalik, C. Nguyen, and H. Al-Ansary, 2016, On-Sun Testing of an Advanced Falling Particle Receiver System, *Solarpaces 2015: International Conference on Concentrating Solar Power and Chemical Energy Systems*, **1734**.

[5] Asay-Davis, X.S., P.S. Marcus, M.H. Wong, and I. de Pater, 2009, Jupiter's shrinking Great Red Spot and steady Oval BA: Velocity measurements with the 'Advection Corrected Correlation Image Velocimetry' automated cloud-tracking method, *Icarus*, **203**(1), p. 164-188.

[6] Lee, S., G. Wolberg, and S.Y. Shin, 1997, Scattered data interpolation with multilevel B-splines, *Ieee Transactions on Visualization and Computer Graphics*, **3**(3), p. 228-244.

[7] Kim, K., N. Siegel, G. Kolb, V. Rangaswamy, and S.F. Moujaes, 2009, A study of solid particle flow characterization in solar particle receiver, *Solar Energy*, **83**(10), p. 1784-1793.

[8] Ho, C.K., J.M. Christian, D. Romano, J. Yellowhair, N. Siegel, L. Savoldi, and R. Zanino, 2017, Characterization of Particle Flow in a Free-Falling Solar Particle Receiver, *Journal of Solar Energy Engineering-Transactions of the Asme*, **139**(2).

[9] National Institute for Occupational Safety and Health (NIOSH). *NMAM 0500: Particulates Not Otherwise Regulated, Total, Manual of Analytical Methods (NMAM)*. 1998 [cited 2018; Available from: https://www.cdc.gov/niosh/docs/2003-154/pdfs/0500.pdf.